


3D Direct Simulation Monte Carlo Modelling of the Inner Gas Coma of Comet 67P/Churyumov–Gerasimenko: A Parameter Study

Y. Liao¹  · C. C. Su² · R. Marschall¹ · J. S. Wu² ·
M. Rubin¹ · I. L. Lai³ · W. H. Ip³ · H. U. Keller⁴ ·
J. Knollenberg⁵ · E. Kührt⁵ · Y. V. Skorov⁴ · N. Thomas¹

Received: 19 June 2015 / Accepted: 27 February 2016 / Published online: 9 March 2016
© Springer Science+Business Media Dordrecht 2016

Abstract Direct Simulation Monte Carlo (DSMC) is a powerful numerical method to study rarefied gas flows such as cometary comae and has been used by several authors over the past decade to study cometary outflow. However, the investigation of the parameter space in simulations can be time consuming since 3D DSMC is computationally highly intensive. For the target of ESA's Rosetta mission, comet 67P/Churyumov–Gerasimenko, we have identified to what extent modification of several parameters influence the 3D flow and gas temperature fields and have attempted to establish the reliability of inferences about the initial conditions from in situ and remote sensing measurements. A large number of DSMC runs have been completed with varying input parameters. In this work, we present the simulation results and conclude on the sensitivity of solutions to certain inputs. It is found that among cases of water outgassing, the surface production rate distribution is the most influential variable to the flow field.

Keywords Direct simulation Monte Carlo (DSMC) · Comets · Coma · Comet 67P/Churyumov–Gerasimenko

✉ Y. Liao
ying.liao@space.unibe.ch

¹ Physics Institute, University of Bern, Bern, Switzerland

² Department of Mechanical Engineering, National Chiao Tung University, Hsinchu City, Taiwan

³ Institute of Space Science, National Central University, Taoyuan City, Taiwan

⁴ Max Planck Institut für Sonnensystemforschung, Göttingen, Germany

⁵ DLR, Institute of Planetary Research, Berlin, Germany

1 Introduction

Often referred to in the past as dirty snowballs, cometary nuclei are considered of major importance in the study of the formation and evolution of the solar system. They consist of dusty grains and icy volatiles which are probably residues of the protoplanetary disk. Direct observations of cometary nuclei from the ground are difficult because of their small size and the partial obscuration by the cometary coma which develops as the comet approaches the Sun. The cometary coma, which can be observed much better, is interesting because it arises from sublimation of frozen volatiles at the surface of the nucleus.

As the development of ESA's Rosetta mission started, it became clear that the coma and the physics of the outflow immediately above the surface needed to be understood. Low production cases at high heliocentric distances needed to be investigated for comparison with early observations. In these cases, the fluid assumptions begin to break down. In particular in the near-nucleus region, ice sublimating into vacuum forms a non-equilibrium boundary layer, the "Knudsen layer" (Kn-layer), with a scale height of ~ 20 mean free paths (mfp) (Ytrehus 1975). Within this region, the velocity distribution function (VDF) can be strongly non-Maxwellian. When Rosetta encountered comet Churyumov–Gerasimenko (C–G), the mfp was of the order of meters to kilometers (Skorov and Rickman 1999; Tenishev et al. 2008) depending upon the distribution of activity across the surface. Using the conventional definition of the Knudsen number (Kn)

$$\text{Kn} = \frac{\lambda}{r}$$

where λ is the mfp and r is the characteristic size (e.g. the nucleus radius), we obtain values of $\text{Kn} < 0.01$ at perihelion for comet C–G and $\text{Kn} > 0.1$ above low activity areas at higher heliocentric distances such as 3.5 au (see e.g. Lai et al. 2015). The rapid decrease in density ($\sim 1/R^2$ where R is the distance to the nucleus) as the gas expands leads to Kn increasing well into the domain of non-equilibrium flows a few kilometers above the surface.

Rarefied gas flows can be described by the Boltzmann equation yet it is difficult to solve. As stated above, analytical solutions using the fluid approach cannot be applied to the regimes of gas flow which are characterized with large Knudsen numbers. Direct simulation Monte Carlo (DSMC) method (Bird 1994), however, provides plausible solutions with the statistical approach for all regimes of gas flow. The basic idea of this technique is to represent many real gas molecules by a few model particles and apply statistical collision models to them. The gas parameters such as density, velocity, and temperature are obtained by averaging the properties of the particles in sampling cells. It has been shown that the DSMC method converges to the Boltzmann equation in the limit of many simulation particles (Nanbu 1980; Wagner 1992). Combi and Smyth (1988) first studied the DSMC approach for comets and, later, 2D axially symmetric DSMC coma models have been published by several authors (Zakharov et al. 2009; Tenishev et al. 2008, 2011; Skorov et al. 2004, 2006; Crifo et al. 2002, 2003, 2005). Skorov et al. (2006) studied Kn-layer gas flows from rotationally symmetric geometries other than simple spheres (spherical sources were considered in Skorov et al. 2004) but only for a 1 au case. Tenishev et al.'s (2008) model includes a kinetic description of the boundary layer, but they did not concentrate on this region in particular and only considered simple spherical geometries for the nucleus. As their aim was to simulate the entire cometary atmosphere, they needed to include physical processes that are irrelevant for the boundary layer. This made sensitivity studies of this region impractical. Fougere et al. (2013a) have used the Tenishev model for their calculations of the outgassing of comet

Hartley 2 and have reported that they have extended the Tennishev et al. code into 3D (Fougere et al. 2013b). The combination of a realistic 3D boundary layer simulation (including inhomogeneous outgassing) with a plausible description of the gas drag coefficient on the dust is the next step in improving the accuracy of coma models and is most probably needed to connect dust distributions observable with Rosetta's OSIRIS imaging system (Keller et al. 2007) to nucleus surface processes.

The DSMC program used here is PDSC⁺⁺ (Su 2013) which is based on the PDSC code developed by Wu and co-workers (Wu and Lian 2003; Wu and Tseng 2005; Wu et al. 2004). PDSC⁺⁺ allows a simulation of 2D, 2D-axisymmetric, and 3D flows on hybrid unstructured grids. The code has been parallelized allowing a much large number of cells and has been implemented on several clusters in Bern and Taiwan. The code is especially useful in that it is able to treat large density gradients by implementation of a variable timestep and a transient adaptive sub-cell technique to increase computational speed and accuracy in the regions of high density (Finklenburg et al. 2014). One should note that as the comet moves towards perihelion, the production rate is expected to climb quite rapidly. For DSMC calculations, the ratio of the mean collision separation (which is the average distance between the collision partners) to the mfp is, in general, required to be close to 1 (Gallis et al. 2008). This can be problematic because it implies a very fine mesh and resulting larger number of cells for the calculation to be executed accurately. For highly active regions, this can drive the calculation beyond available resources. However, the parallelization computing and the computation on Graphic Processor Units (GPUs) can increase the performance dramatically (Su et al. 2012). Finally, it should be recognized that most calculations to date have been steady-state (Combi 1996 being an exception). As discussed in Sect. 3, this is almost certainly adequate for most cases although there is little doubt that modelling of transient events within the cometary coma will provide further strong constraints on the outflow. However, the computational cost of such studies in 3D is likely to be enormous unless significant simplifications can be made.

The aim of this work is to identify to what extent modification of selected parameters influence the 3D gas flow fields and to establish the reliability of inferences about the initial conditions from in situ and remote sensing measurements. To do this, we have completed a large number of DSMC runs with varying input parameters. We make this relevant by using test cases which would be appropriate estimates for the outgassing from comet Churyumov–Gerasimenko (C–G) using a non-axisymmetric shape model of the nucleus of the comet obtained from in situ observations by OSIRIS onboard Rosetta (Jorda et al. 2015) and now publicly available.

The remainder of the text is separated into the following sections. Section 2 describes the physics assumed for the models, the numerical assumptions and the boundary conditions we have used to initialize the calculations. Section 3 illustrates the results and is split into sub-sections which correspond to different cases which we have run. In all cases, we have attempted to isolate the effects resulting from changes in the initial conditions. We conclude with the usual discussion and conclusions section.

2 Models

The flow chart shown in Fig. 1 illustrates our modelling approach for the inner gas and dust coma of C–G. The first three models (shape model, thermal model, and gas dynamics variables) drive the gas dynamics in the rarified gas dynamics model which serves as the

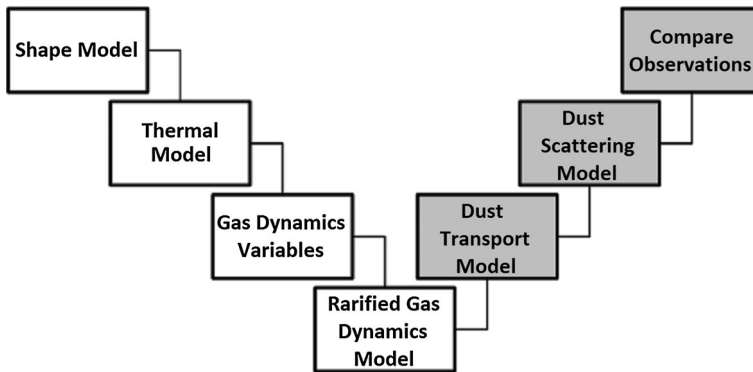


Fig. 1 The modelling approach (going from *left to right*) which we adopt for the simulation. Dust models and the comparison with observations marked in a *grey tone* will not be presented in this work

input for the dust models thereafter. As this paper focuses on the gas coma, details of the first three models will be described in the sub-sections below and the last model will be presented as the results. The dust component of the scheme will be presented elsewhere. The approach we have chosen is both extremely flexible and computationally fast. Nonetheless, certain assumptions are necessary and, in some cases, desirable since there is no need to introduce additional complexity if it can be shown to be of little importance. Other assumptions, however, may influence the results but the absence of precise knowledge of parameters (e.g. molecular parameters) implies that we must state our assumptions and assess the associated errors.

2.1 Simulation Region and Shape Model

The primary region of interest for Rosetta experiments is in the innermost coma. It is generally assumed that the gas distribution in this region will help constrain the surface properties. Beyond this region, there is a region of essentially free radial outflow for which the physics is reasonably well understood and which provides only limited constraints on the surface properties. The region covered by a DSMC simulation can be manipulated by adaptation of the grid. However, typically we are studying regions up to around 5 nuclear radii from the surface. If we assume, very conservatively, a constant gas outflow velocity of around 200 m/s then the gas outflow will reach the edge of the simulation region in timescales of the order of a minute (for a 2 km radius nucleus). Higher velocities expected when closer to the Sun would imply even shorter timescales. Furthermore, although transient solutions to dynamic processes are interesting, the basic problems to be addressed can probably be handled by studying steady-state solutions. For this assumption to hold, changes in the outflow should not occur on timescales shorter than around 1 min, which given the comparatively slow rotation of the nucleus (12.4 h for CG; Mottola et al. 2014) is a fairly straightforward assumption for the gas phase.

We use a public shape model of the nucleus of the comet released by ESA (Jorda et al. 2015) to provide the surface boundary condition. This model has 62,908 facets with a total surface area of 39.3 km². The radius of the nucleus is around 2.1 km on the x–y plane (Fig. 2). The dimensions of the surface facets are interpolated to be comparable to the mfp when C–G is around perihelion. The simulation domain extends out to 10 km from the

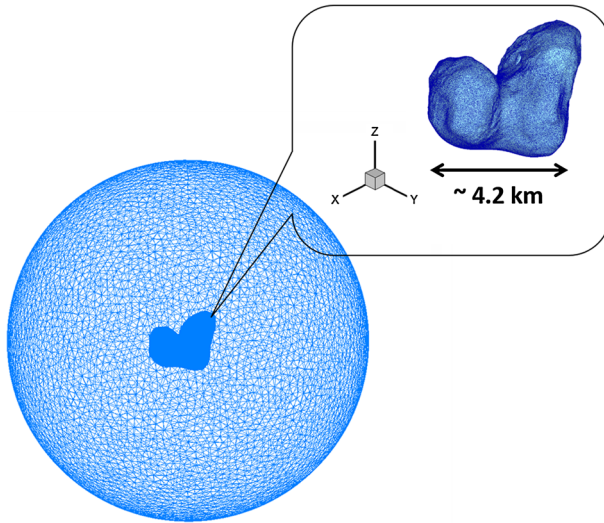


Fig. 2 The 3D public shape model of C–G (SHAP2) and the unstructured grid showing the simulation domain

center of the nucleus and the outer edge of the domain is assumed to be a vacuum boundary. The rotation axis of C–G is the z axis of the model.

2.2 Sublimation Process and Thermal Model

The sublimation process is not well understood. Poorly constrained physical parameters such as the thermal inertia and the depth of the emitting surface have an impact on the sublimation flux and the velocity of escaping gas molecules. Sub-surface sublimation through a high temperature porous surface may be important (Skorov and Rickman 1995). Ices of different volatility may sublime from different depths. Sublimation models of significant complexity have been published trying to address many of these issues (Huebner et al. 2006). Here we need to produce an initial boundary condition realistically for tens of thousands of facets. As noted above, observations point towards a very low thermal inertia (e.g. Groussin et al. 2013) and consequently, the simplest realistic possibility would be to use an energy balance equation with no thermal inertia for a pure (but dark) water ice surface in equilibrium (with vanishing time derivative), i.e.

$$0 = \frac{S(1 - A_H) \cos i}{r_h^2} - \varepsilon\sigma T^4 - L \frac{dm}{dt}$$

where S is the solar constant at 1 au, r_h is the heliocentric distance in (au), A_H is the surface hemispheric albedo (bond albedo), i is the angle of solar incidence, ε is the IR emissivity, L is the latent heat of sublimation of H_2O , dm/dt is the mass loss rate caused by sublimation, σ is Stefan-Boltzmann's constant, and T is the surface temperature.

Clearly, a model generating a specific production rate/velocity distribution via a more sophisticated approach might be produced elsewhere and could subsequently be entered into the DSMC model. However, the output from such a model should be simplified since the DSMC resolution and modelling limitations imply a limit to the fidelity of the final

model which may not be justified. Specifically, boundary conditions should be adapted to the length scales of the surface grid dimension.

With the equation alone we would produce a model with a sublimation rate around 2 orders of magnitude higher than observed. We compensate for this by using the concept of an active fraction for each facet. In other words, a large fraction of each facet is assumed to be completely inert with the fractional area active being manipulated to match the observed production rate.

2.3 Gas Dynamics Variables

2.3.1 Initial Rotational Temperatures and Non-local Thermal Equilibrium

Water vapour has 6 degrees of freedom (DOF). The initial distribution of energy in these DOF at source is essentially unknown. Release from a pure ice surface provides translational energy to the molecules but only post-collision energy is transferred to the rotational DOF. Passage of gas through a porous structure at higher density may lead however to rapid equilibrium prior to or immediately after release. Hence this requires significant assumptions. Here we assume that the initial translational and rotational temperatures are identical (i.e. we already have equilibrium at source).

There are numerous processes which can affect the temperatures of gas molecules in the vicinity of the nucleus (Lee et al. 2011). For the purposes of this work, we will ignore processes such as water-electron collisions, which can influence the rotational temperatures of water molecules, because of the dominance of the rate coefficient for water–water collisions.

2.3.2 Collision Models

A key aspect required to perform DSMC calculations is the molecular model that specifies the interaction between the colliding species (Alexeenko, abstract, DSMC13, 2013). While recognizing recent developments in more detailed molecular models, we adopt here a standard variable soft sphere (VSS) model because of its computational efficiency and its accuracy with regards to viscosity using only a limited parameter set. The differences between variable hard sphere (VHS) and VSS models are known to be rather small. Examples are given in Vargas et al. (2011) and Finklenburg (2014). Differences when using the hard sphere model or a Maxwellian intermolecular potential were also noted in these papers and might be investigated although we expect the consequences for cometary outflow to be small.

2.3.3 Outgassing Forms

Here we define two outgassing forms, homogeneous and inhomogeneous, as one of the major concerns in the initial boundary conditions. For the homogeneous case, the thermal model has been run to compute the production rate from each facet and it is here assumed that the whole nucleus is potentially active. For the inhomogeneous case, an activity pattern has been constructed. We use as a basis, the homogeneous case result but numerically restrict outgassing to specific areas on the surface which we define in an ad hoc manner. The area definition has been chosen to test various effects within one model

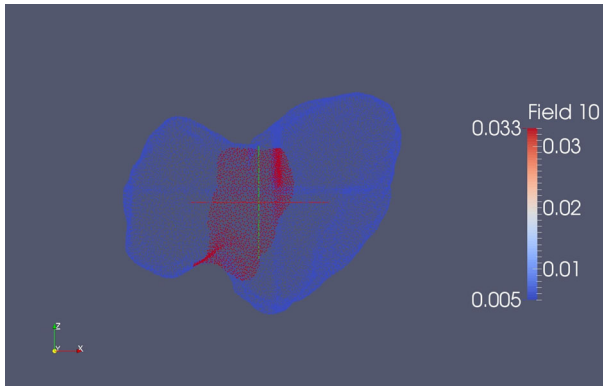


Fig. 3 The increased active fraction has been applied in the neck region by a factor of 6.5 relative to the rest of the nucleus for the inhomogeneous case

run. The defined active areas are shown in Figs. 3 and 4 demonstrates the resulting distribution of subliming flux.

2.3.4 Initial Velocity Distribution Functions

The initial velocity distribution function (VDF) of the gas at the surface of the nucleus is determined physically by a vast number of variables that are essentially unknown. We adopt two methods for describing the initial VDF. Firstly, we assume that a half-Maxwellian velocity distribution at a given temperature of the surface is sufficient to specify the initial conditions. A key aspect will be to establish whether breaking this assumption with an alternative has any measureable effect on the outflow. Our second approach is to use a cosine law such that the normalized angular distribution is given by

$$f(\theta) \propto \cos^n(\theta)$$

where n is an exponent ($n \geq 1$) and θ the angle to the surface normal. This takes into account the comments by Greenwood (2002) on the correct construction of the boundary condition.

2.3.5 Reflecting or Absorbing Boundaries

One additional aspect became important during the investigation of cases. That is the back flux of the gas and how reflected gas molecules (molecules which, through collisions, return to the surface) are treated. The idea of recondensation on the nightside of the nucleus (equivalent to an absorbing boundary) was discussed by Rubin et al. (2014). We have chosen to set the nucleus as an absorbing surface for most cases in this paper but also show a test case with a reflecting surface. This not only implies that the net flux from the surface is reduced but the reduction is dependent upon the initial velocity distribution function. Cosine distributions with a high value of n will have a higher net flux from the surface than a half-Maxwellian initial VDF. The effect of this will be illustrated below.

It should be noted that the flow back to the nucleus reduces the total outflow below that given by the energy balance equation and hence self-consistency is lost. Energy is also

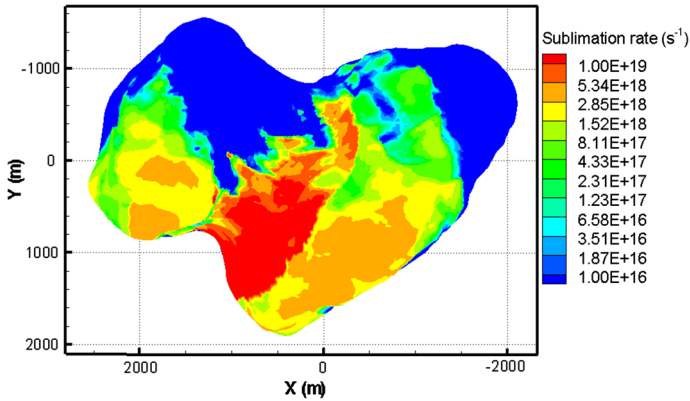


Fig. 4 The sublimation rate at the surface for the orientation that we study herein resulting from the inhomogeneous activity distribution seen in Fig. 3

deposited through re-condensation. This would need to be taken into account in a physically correct manner in a more sophisticated model of the boundary conditions.

2.3.6 Compositions

It is assumed that gases other than H_2O , CO_2 , and CO are trace species which have no influence on the flow properties. We have assumed that H_2O is the dominant species. However, CO_2 and CO can also be implemented and their relative number densities can be modified in the DSMC simulations. We assume that the comet are equipped with H_2O and CO_2 but depleted in CO and have studied relative number densities $\text{H}_2\text{O}:\text{CO}_2 = 3:1$ (e.g. Fig. 4 in Hässig et al. 2015) to establish possible effects of the multi-species outgassing.

One of the intriguing possibilities is that different active regions may have different compositions (Hässig et al. 2015). The investigation of this is complicated by gas jet interactions. Finklenburg (2014) ran a series of simple DSMC models in 2D to study the effects of jet interactions and showed how mixing of CO_2 and H_2O is a strong function of the Knudsen number. This is fairly simple to explain in that, for low production rates, the number of collisions is small and hence the interacting jets penetrate each other. For an orbiting spacecraft it becomes increasingly difficult to identify the relative compositions of the two sources as the production rate drops. For high production rates, collisions limit the interaction such that the molecules from the different sources are much more clearly separated spatially even at large distances from the nucleus.

For this work, the composition of the gas coma will be an input parameter as we seek to establish the influence of one gas on the other for simple test cases.

3 Results

The cases investigated are shown in Table 1. For our primary study case, we have placed C–G at a heliocentric distance of 3.4 au with a gas production rate around 1.25 kg/s based on MIRO measurements (Gulkis et al. 2015). Homogeneous outgassing is set as a standard outgassing form but two cases with inhomogeneous outgassing are also performed for

Table 1 Parameters used in our models for test cases

Case	Outgassing form	R_h (au)	Q (kg/s)	Composition	VDF	Z_{rot}	Surface type
0 ^a	Homogeneous	3.4	1.25	100 % H ₂ O	½ M–B	1	100 % abs.
1	Inhomogeneous	3.4	1.50	100 % H ₂ O	½ M–B	1	100 % abs.
2	Homogeneous	1.3	19.4	100 % H ₂ O	½ M–B	1	100 % abs.
3 ^b	Homogeneous	3.4	1.25	100 % H ₂ O	$\cos^n(\theta)$	1	100 % abs.
4	Inhomogeneous	1.3	22.9	100 % H ₂ O	½ M–B	1	100 % abs.
5	Homogeneous	3.4	1.43	75 % H ₂ O 25 % CO ₂	½ M–B	1	100 % abs.
6	Homogeneous	3.4	1.25	100 % H ₂ O	½ M–B	8	100 % abs.
7	Homogeneous	3.4	1.25	100 % H ₂ O	½ M–B	1	100 % ref.

The outgassing form (homogeneous or inhomogeneous), the heliocentric distance R_h (au), the gas production rate Q (kg/s), the VDF (velocity distribution function: half-Maxwellian or cosine law distribution), the composition of the gas (pure H₂O gas or mixing gas of H₂O and CO₂), the rotational relaxation collision number Z_{rot} and the surface type (totally absorbing or reflecting) are given

^a Case 0 is designed as a standard case

^b Since our DSMC code allows implementations of the cosine law distribution with the power n from 1 to 9, all 9 cases have been investigated but summarized as 1 case in the table

comparison. One should note that the production rates of the inhomogeneous cases are slightly higher.

We assume the albedo A_H to be 0.04. As this enters in the thermal balance equation as $(1 - A_H)$, even significant changes to A_H have relatively little influence on the results. The thermal emissivity ϵ has been set to the canonical value of 0.9. Here, other values can have larger differences in terms of total gas production. A half Maxwell–Boltzmann initial velocity distribution function has been selected as a standard case but cases with cosine law distributions ($n = 1-9$) have also been studied. Surface sublimation, pure water ice as the gas source, and a rotational relaxation collision number of 1 have also been adopted as standard. We shall investigate variations with respect to several of these parameters.

The initial boundary conditions of each case are shown in figures below. Figure 5 shows the temperature distribution of sublimating surfaces for all the simulation cases. As the result of thermal model, these temperatures are low because sublimation acts to keep the

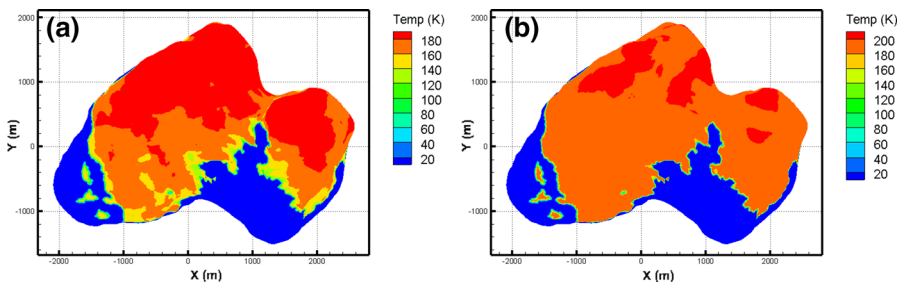


Fig. 5 Initial temperature distributions upon the nucleus surface of **a** low production rate cases (Case 0; Case 1; Case 3; Case 5; Case 6; Case 7) and **b** high production rate cases (Case 2; Case 4). Note that the two pictures are with different scales

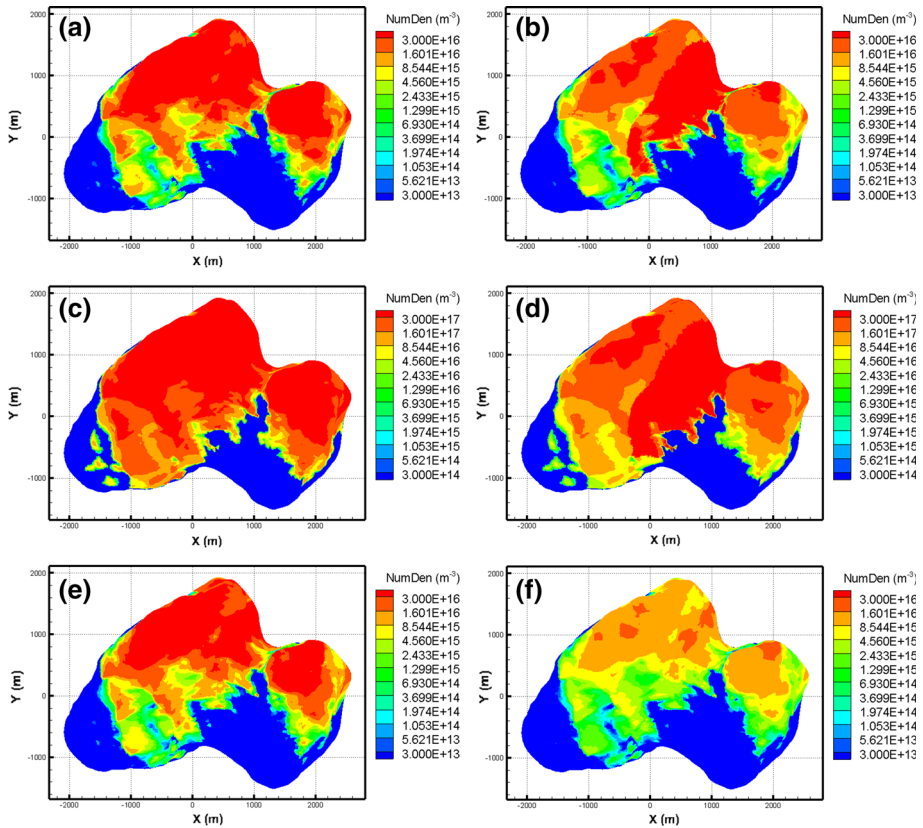


Fig. 6 Initial number density distributions upon the nucleus surface of **a** Case 0; Case 3; Case 6; Case 7, **b** Case 1, **c** Case 2, **d** Case 4, **e** Case 5: H₂O, **f** Case 5: CO₂. Note that the scale of **c** and **d** is 1 order of magnitude higher than the scale of all other cases

temperature down to ~ 185 K. It should be noted here that we do not discuss the temperature of the inactive fractional area of the surface as this is assumed not to have any influence on the calculation. This is, however, a significant assumption because collisions of molecules with the inactive surface may be a source of heat for the gas.

Figure 6 shows the number density distributions at the nucleus surface also obtained from the thermal model. Outgassing results corresponding to these boundary conditions are displayed and discussed in sub-sections below.

3.1 Outgassing Forms and Production Rates

Figure 7a (Case 0) represents the standard case with homogeneous water outgassing in response to solar insolation. The total production rate in the chosen (default) orientation is 1.25 kg s^{-1} . Figure 7b (Case 1) is the case with inhomogeneous outgassing and a slightly higher production rate of 1.5 kg s^{-1} . In general, the number density decreases with the distance to the nucleus as expected. Case 1 shows a more focussed distribution pattern of gas molecules on the dayside of C–G compared to Case 0. However, at the outer boundary

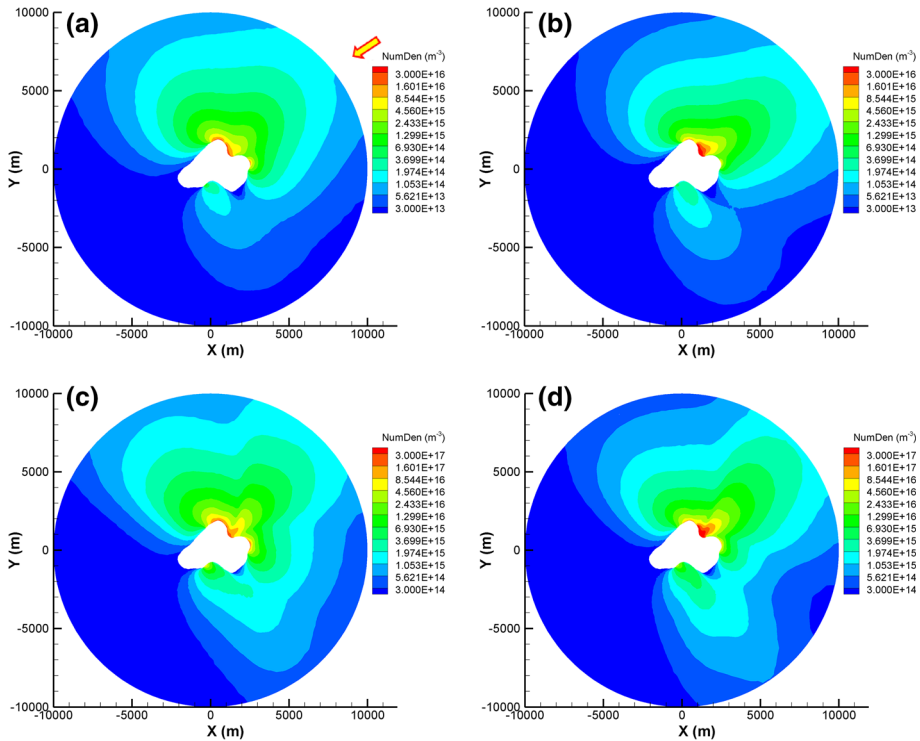


Fig. 7 Number density distributions of the inner gas coma of **a** Case 0, **b** Case 1, **c** Case 2, and **d** Case 4. Note that the scale of **c** and **d** is 1 order of magnitude higher than the scale of **a** and **b**. The *arrow* marked in **a** indicates the direction of insolation projected on the x - y plane

of the simulation region (10 km), the effect of gas concentration caused by inhomogeneous outgassing is less obvious. This illustrates clearly that the signature of inhomogeneous outgassing in the local number density becomes rapidly weaker with come to centric distance. Figure 7c, d (Cases 2 and 4) are identical to Case 0 and Case 1 but with the comet at perihelion (~ 1.3 au). It is important to note here that this is not physical in the sense that the sub-solar latitude changes in reality. Our test cases here are simply showing what would happen if the comet were transported to 1.3 au with all other parameters remaining unchanged. The cases show higher number densities as a result of the initial boundary conditions, but again the difference between homogeneous and inhomogeneous gets less significant as the distance to the nucleus increases. The inhomogeneities are however visible further out from the nucleus. Note, also, the stronger interaction between the jets (in particular, at an azimuth of around 140 degrees clockwise from the vertical).

The gas bulk velocities in the inner coma are shown in Fig. 8. With all the plots it is clear that the velocity increases with distance to the nucleus and gas can be accelerated to supersonic speeds within a short distance from the nucleus. Figure 8b (Case 1) indicates that the velocity increases more rapidly above the local active areas. Figure 8c (Case 2) and d (Case 4) also show a rapid increase of velocity at most places within the simulation region because of the higher production rates set in the initial boundary conditions. The

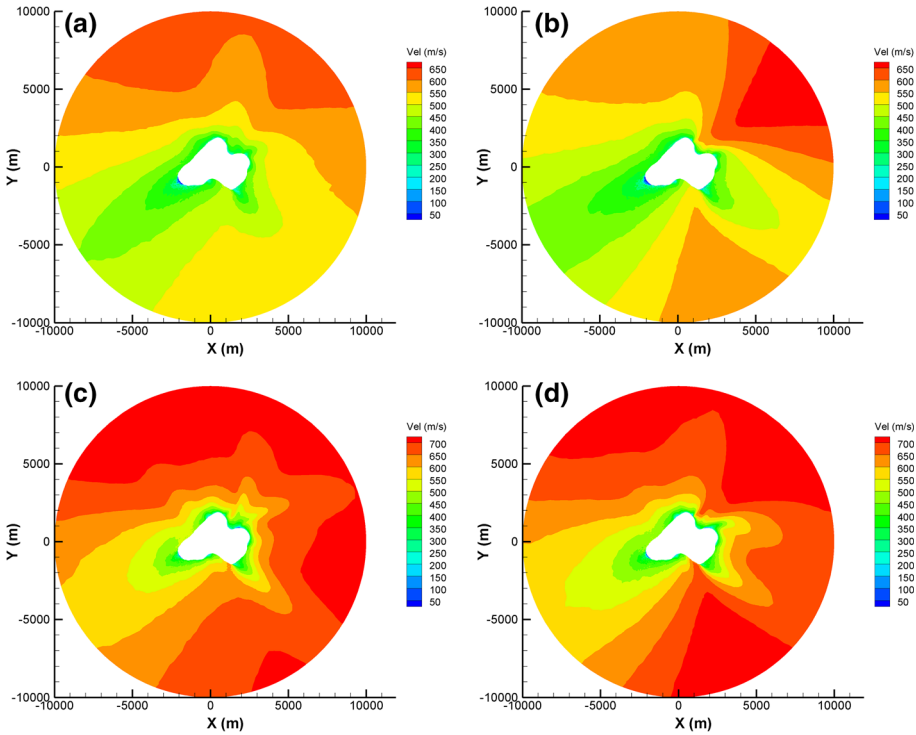


Fig. 8 Velocity distributions of the inner gas coma of **a** Case 0, **b** Case 1, **c** Case 2, and **d** Case 4

local influence of jets is stronger and we would therefore predict more rapid changes in outflow speed for a fast fly-through of these structures at perihelion. Figure 9 shows the total temperature distributions as the average of the translational and the rotational temperatures. The temperature decreases as the velocity increases because of the adiabatic expansion of the gas. Comparing to Fig. 9a (Case 0) and Fig. 9b (Case 1), Fig. 9c (Case 2) and Fig. 9d (Case 4) show fast decreases of the temperature and cooler gas comae because of more collisions and thus more energy transfer.

Figure 10 shows the ratio of the rotational temperature to the translational temperature ($T_{\text{rot}}/T_{\text{trans}}$) which defines the non-local thermal equilibrium (non-LTE) in the coma. Figure 10a, b (Case 0 and 1) show that only regions close to local active areas are in equilibrium and it should be noted that this was set as the initial boundary condition. Hence, the gas moves away from LTE in the 3.4 au cases and at the outer boundary (10 km from the nucleus centre and close to the minimum distance above the nucleus Rosetta reached) we see non-LTE independent of position. The ratios in Fig. 10c, d are closer to 1 on the dayside of the nucleus indicates that the gas coma is closer to local thermal equilibrium (LTE) as might be expected.

3.2 Velocity Distribution Function

In Case 3, the initial VDF has been changed to cosine law distributions for n from 1 to 9. As shown in Fig. 11, the number density distributions do not show major differences between the cosine law distributions (Fig. 11b–d) and the half Maxwellian distribution

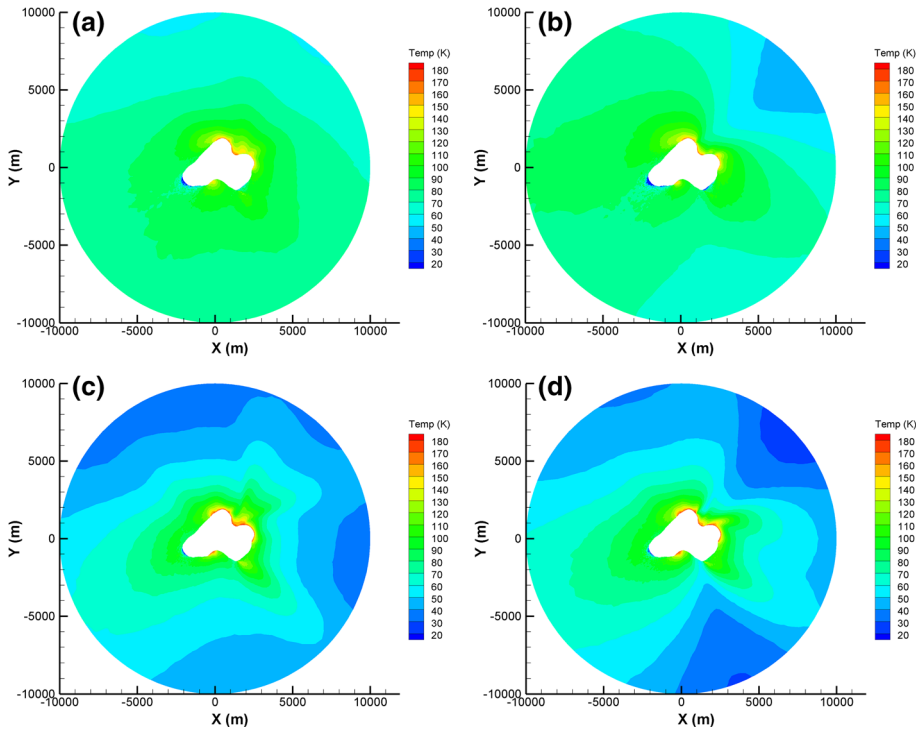


Fig. 9 Total temperature distributions of the inner gas coma of **a** Case 0, **b** Case 1, **c** Case 2, and **d** Case 4

(Fig. 11a). There is some indication of increased collimation as n increases but this would hardly be discernible in measurements of gas density by Rosetta. However, significant changes can be seen in both the velocity (Fig. 12) and temperature (Fig. 13) distributions.

Figure 12 shows that for the Maxwellian–Boltzmann VDF (Case 0; Fig. 12a), the velocity at the edge of the flow field is slightly higher than the one for the cosine law VDF (Case 3; Fig. 12b–d). This leads to the slightly lower number densities at the outer boundary of the simulation region (10 km) seen in Fig. 11a although this is hard to observe in a logarithmic display. The reason for this can be seen in Fig. 13 where the temperatures are slightly higher in the M–B case. In Fig. 13, the temperature at the outer boundary drops as number density increases. With large n in $\cos^n(\theta)$ the gas outflow automatically ends up with a higher bulk velocity and a lower thermal temperature because the lateral motion of the gas is suppressed. The increased collimation of the source appears to require more energy from the gas to move towards local thermal equilibrium.

The extent of collimation of the gas can also be observed in the distributions of the temperature ratio. From Fig. 14a (Case 0) and (b) (Case 3: $n = 1$), it is clear that the area close to LTE is larger with a cosine law distribution than the M–B distribution. For cosine law VDF cases, we can see that the area increases as the power of cosine law increases by comparing Fig. 14b (Case 3: $n = 1$) and Fig. 14c (Case 3: $n = 5$). However there is no significant difference between Fig. 14c (Case 3: $n = 5$) and Fig. 14d (Case 3: $n = 9$).

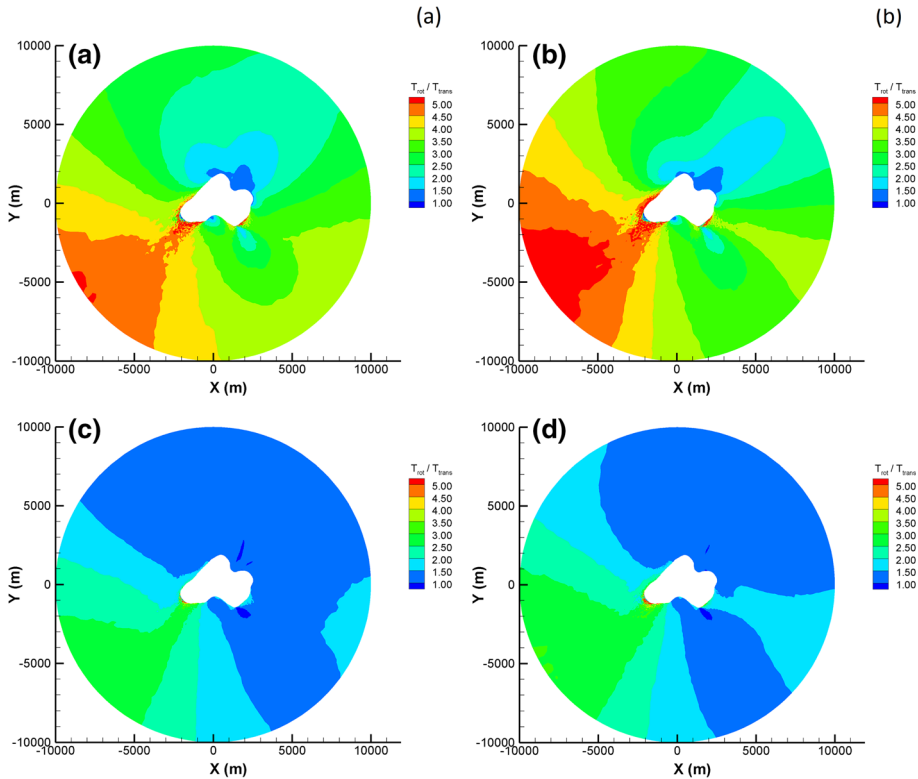


Fig. 10 Temperature ratio (T_{rot}/T_{trans}) distributions of the inner gas coma of **a** Case 0, **b** Case 1, **c** Case 2, and **d** Case 4

3.3 Rotational Relaxation Collision Number (Z_{rot})

This value defines how many collisions are required to redistribute energy on the various DOFs. Figure 15 shows a comparison between cometary comae with different rotational relaxation collision numbers (Z_{rot}). Figure 15a (Case 0) is the case with $Z_{rot} = 1$ while Fig. 15b (Case 6) is with $Z_{rot} = 8$. Figures 16, 17, and 18 show the speed, temperature and temperature ratio of the gas. As can be seen, the influence of Z_{rot} seems insignificant at these low production rates. The reason is that the inner coma is very rarefied and far from equilibrium at 3.4 AU such that even with $Z_{rot} = 1$ cannot fully transfer the rotational energy to the translational one. Therefore, there are no significant changes of the physical properties of the flow field with a much larger rotational relaxation collision number.

3.4 Gas Composition

Case 5 is assumed with a gas mixture of H_2O and CO_2 . As mentioned in Sect. 2.3.6, some assumptions have been made for simplicity. A relative number density $H_2O:CO_2 = 3:1$ has been set and the local active areas are the same for both species. Figure 19 shows how much difference in the amount of the two species by taking a number density ratio

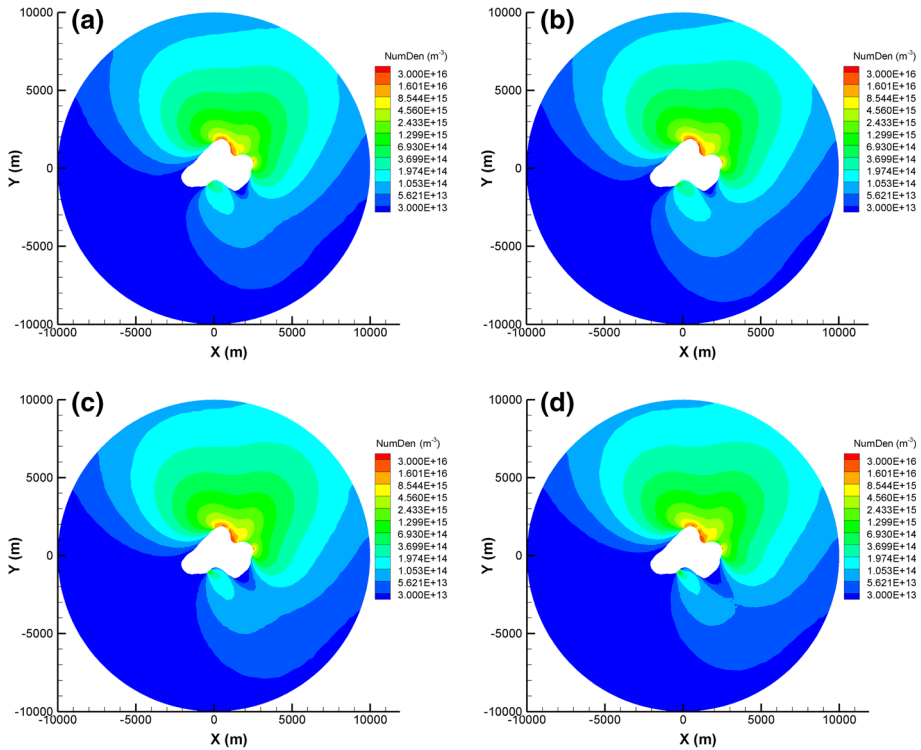


Fig. 11 Number density distributions of the inner gas coma of **a** Case 0, **b** Case 3: $n = 1$, **c** Case 3: $n = 5$, and **d** Case 3: $n = 9$

$N_{\text{H}_2\text{O}}/N_{\text{CO}_2}$. On the dayside the number density ratios are mostly larger than 3.0 because of the assumption of initial number densities. For the velocity distribution shown in Fig. 20, it is evident that CO_2 gas is slower than H_2O because it is heavier. The difference between the total temperature distributions of the two species (Fig. 21) is relatively small compared to the number density and the velocity distributions. This may be explained that CO_2 and H_2O are close to thermal equilibrium and thus they hold similar temperature distributions.

3.5 Reflecting or Absorbing Boundaries

Figures below show comparisons between cometary comae with different surface properties. Figure 22a (Case 0) is the case with an absorbing nucleus surface while Fig. 22b (Case 7) is with a specular reflecting surface. We are aware that the assumption of the 100 % reflecting surface is not realistic and might vary across the surface but still may be useful for testing purposes. For the number density distributions, we can see that there are slightly more gas particles in the flow field of the dayside in Fig. 22b (Case 7) than in Fig. 22a (Case 0). The effects on the flow field caused by a reflecting surface are also small compared to the one of an absorbing surface in terms of the velocity (Fig. 23b), temperature (Fig. 24b) and temperature ratio (Fig. 25b) distributions. The reason may be explained by the low surface temperature. The residence times of molecules relevant for ice surfaces depend on the species and the surface temperature (Sandford and Allamandola

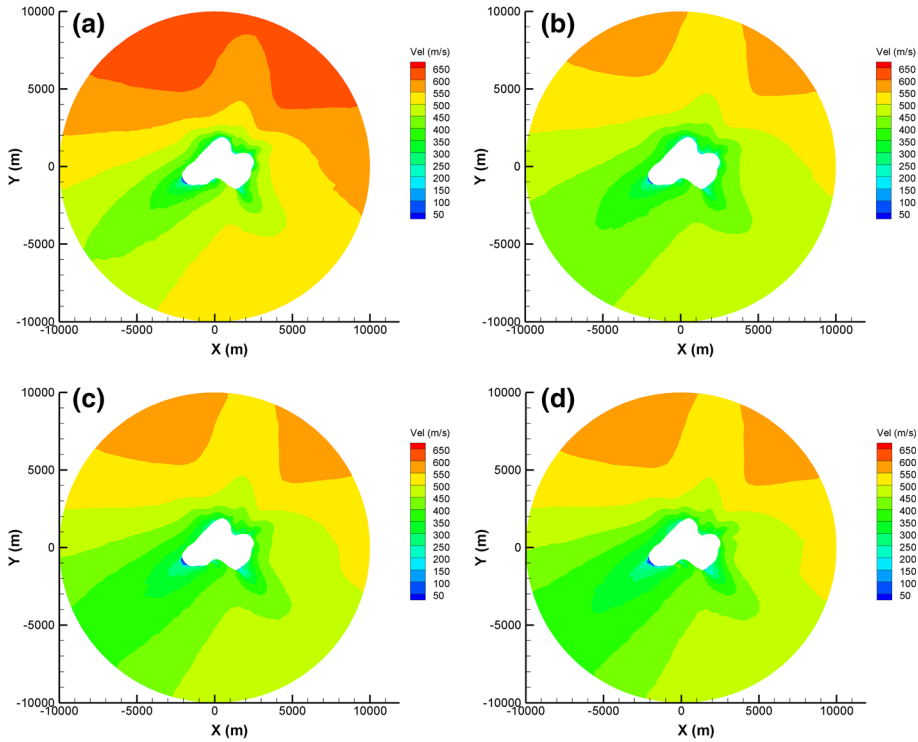


Fig. 12 Velocity distributions of the inner gas coma of **a** Case 0, **b** Case 3: $n = 1$, **c** Case 3: $n = 5$, and **d** Case 3: $n = 9$

1993). At 150 K, the residence time of water molecules on water icy surface is ~ 30 s but it reaches ~ 6300 s at 130 K. As stated in Sect. 2.1, the simulation timescale of our cases is the order of a minute. A reflecting surface would serve as an absorbing surface with the surface temperature below 150 K. Therefore, the outgassing results of a reflecting surface (Case 7) are similar to the results of an absorbing surface (Case 0).

4 Conclusions

Our DSMC code (PDSC⁺⁺) has been used to study various models of the gas outflow from comet C–G. The code uses an unstructured grid and can provide global values for gas density, velocity, and temperature out to 10 km from the nucleus at good resolutions. Predictions for the flow field at 1.3 au under simplified boundary conditions have been presented. We have simulated the gas kinetics in the inner most coma of C–G and identified to what extent modification of parameters influences the gas flow field. For cases of single species outgassing (H_2O), the production rate Q is the most influential parameter. Differences of the gas distributions between homogeneous and inhomogeneous outgassing are evident but would be less clear in the coma 10 km away from the nucleus as the gas

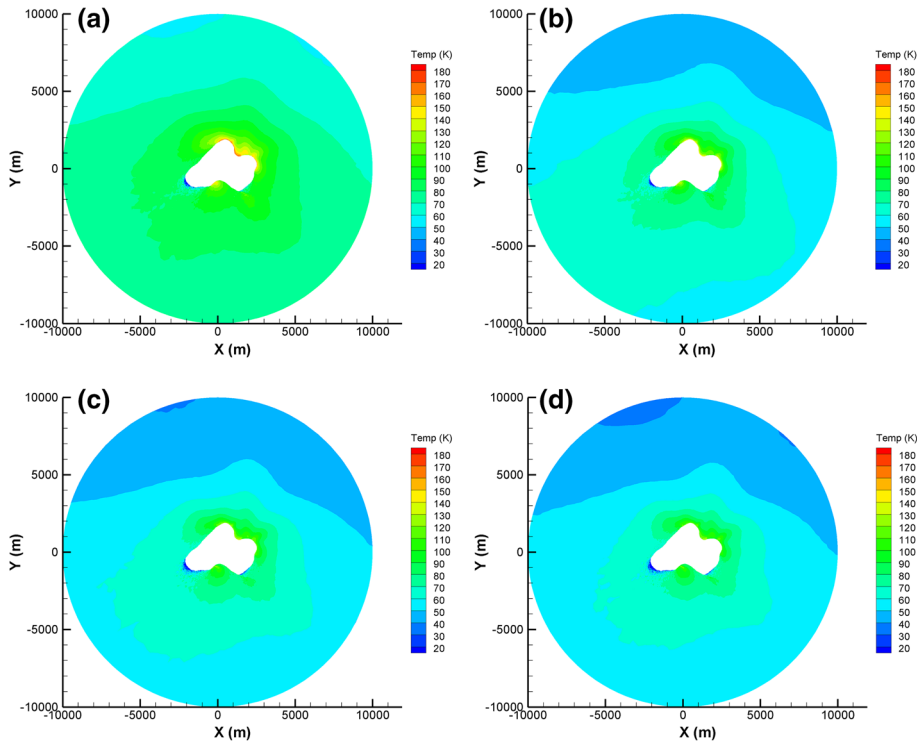


Fig. 13 Total temperature distributions of the inner gas coma of **a** Case 0, **b** Case 3: $n = 1$, **c** Case 3: $n = 5$, and **d** Case 3: $n = 9$

expands. Thus, in order to search for inhomogeneities of outflow it is vital that measurements of gas density and temperature are made close to the nucleus.

The cosine law velocity distribution function imposes some changes in the flow field. The collimation effect of the gas is not easily seen in the number density distributions but clearly evident in the velocity and temperature distributions. In general, the cosine law distribution function should change significantly the flow field of the free molecular flow (Zhang et al. 2012). It is the collisions between the gas particles that may help to explain why the collimation effect resulted from the cosine law distribution is not so strong. The energy is redistributed through collisions and reaches a Maxwell–Boltzmann distribution when the flow field is in equilibrium.

The varying of the rotational relaxation collision number, Z_{rot} , has almost no influence on the coma.

The result of the 100 % reflecting surface on the coma is significant and interesting however unphysical because it resembles a uniform outgassing when the flow field reaches steady state. For cases of multispecies outgassing (H_2O and CO_2), the amount of the two species depends on the initial boundary conditions. As for the velocity distribution, CO_2 is apparently slower than H_2O as expected. More variables will be investigated in the future, and our DSMC code will be compared to measurements obtained by the Rosetta instrumentation, both in situ and remote sensing, using more sophisticated nucleus shape and thermal models.

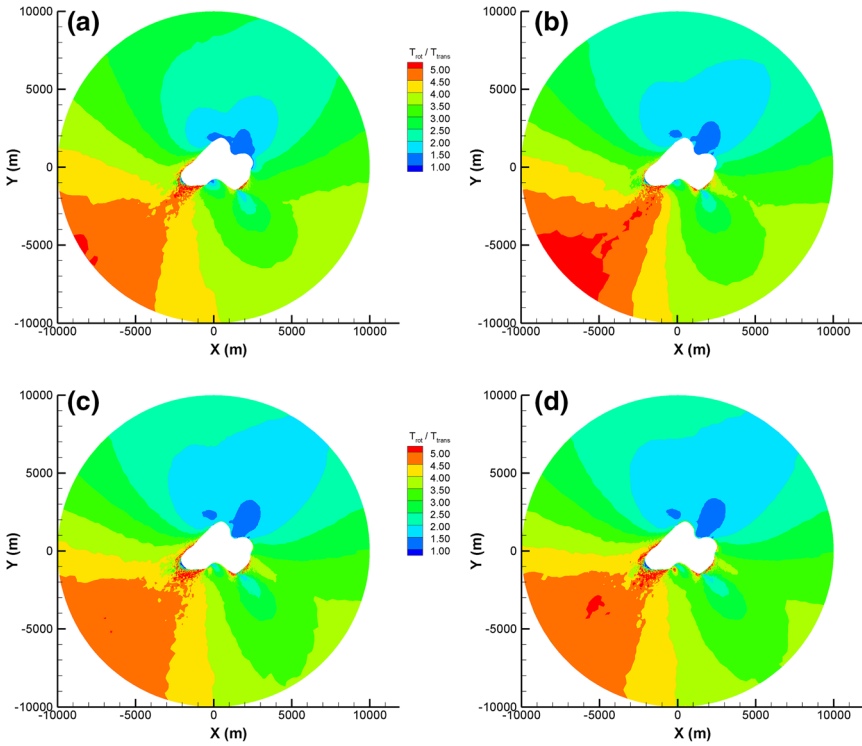


Fig. 14 Temperature ratio (T_{rot}/T_{trans}) distributions of the inner gas coma of **a** Case 0, **b** Case 3: $n = 1$, **c** Case 3: $n = 5$, and **d** Case 3: $n = 9$

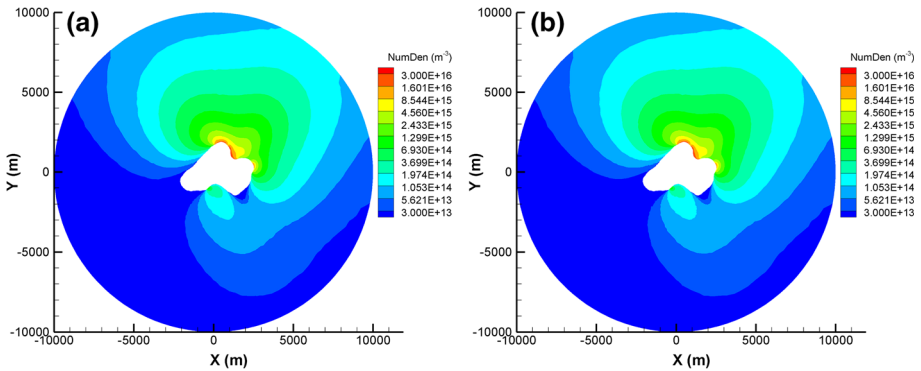


Fig. 15 Number density distributions of the inner gas coma of **a** Case 0 and **b** Case 6

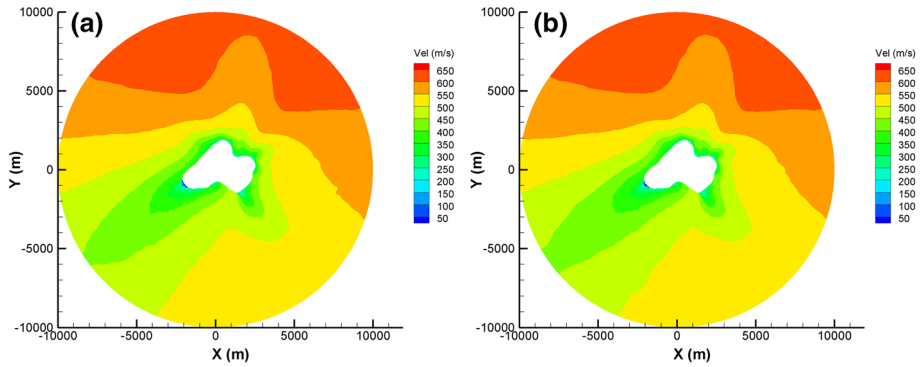


Fig. 16 Velocity distributions of the inner gas coma of **a** Case 0 and **b** Case 6

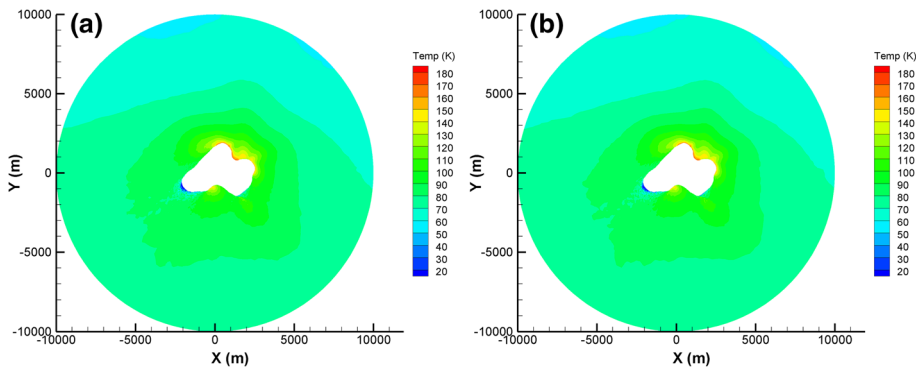


Fig. 17 Total temperature distributions of the inner gas coma of **a** Case 0, and **b** Case 6

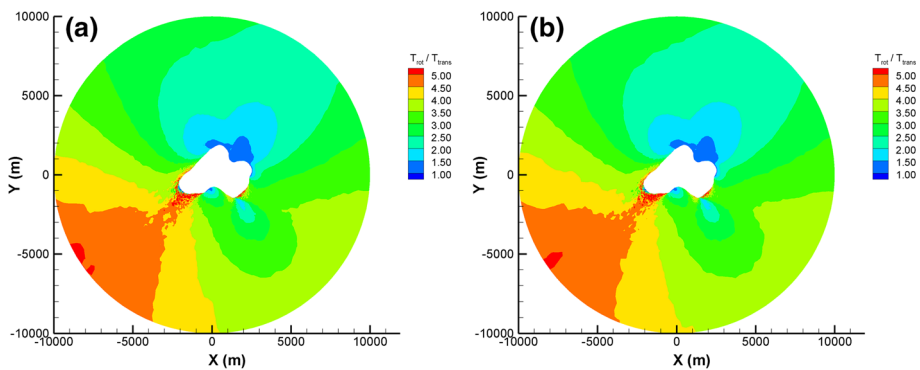


Fig. 18 Temperature ratio (T_{rot}/T_{trans}) distributions of the inner gas coma of **a** Case 0, and **b** Case 6

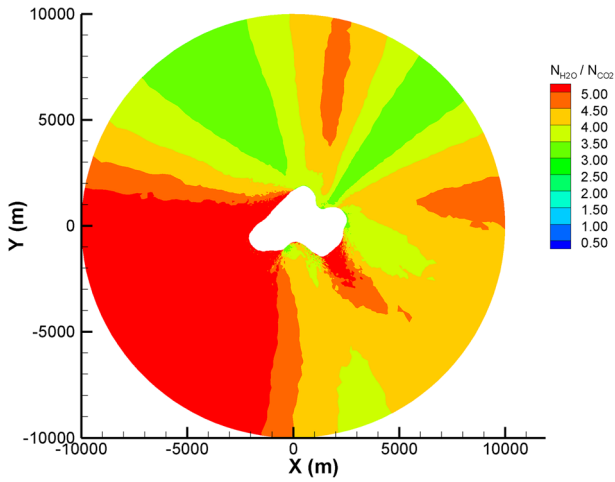


Fig. 19 Number density ratio ($N_{\text{H}_2\text{O}}/N_{\text{CO}_2}$) distributions of the inner gas coma of Case 5

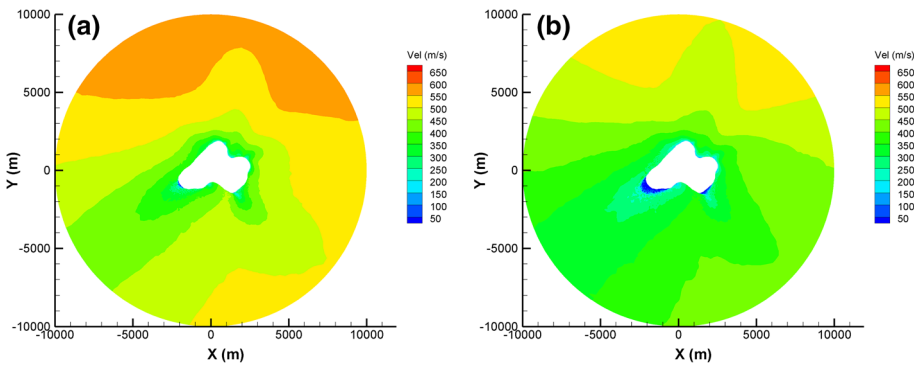


Fig. 20 Velocity distributions of the inner gas coma of Case 5 of **a** H_2O , and **b** CO_2

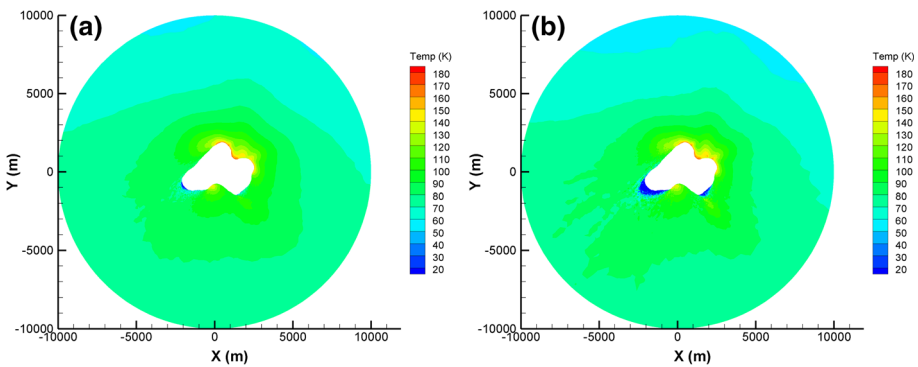


Fig. 21 Total temperature distributions of the inner gas coma of Case 5 of **a** H_2O , and **b** CO_2

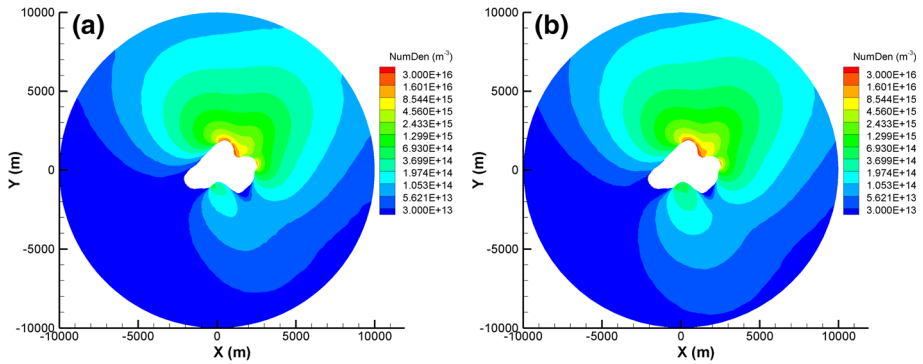


Fig. 22 Number density distributions of the inner gas coma of **a** Case 0, and **b** Case 7

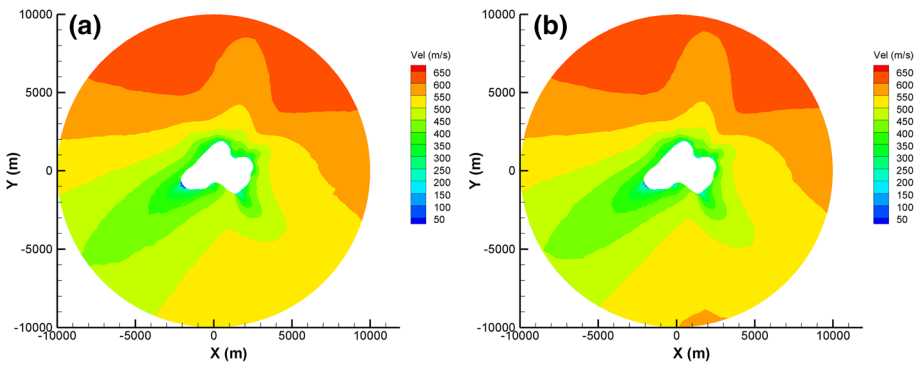


Fig. 23 Velocity distributions of the inner gas coma of **a** Case 0 and **b** Case 7

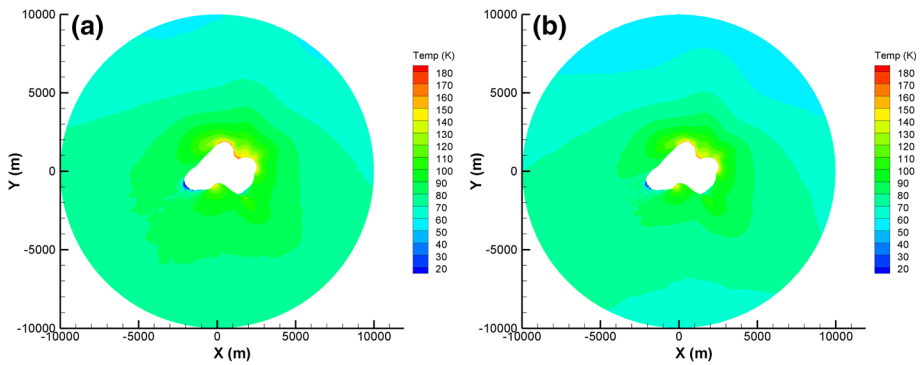


Fig. 24 Total temperature distributions of the inner gas coma of **a** Case 0, and **b** Case 7

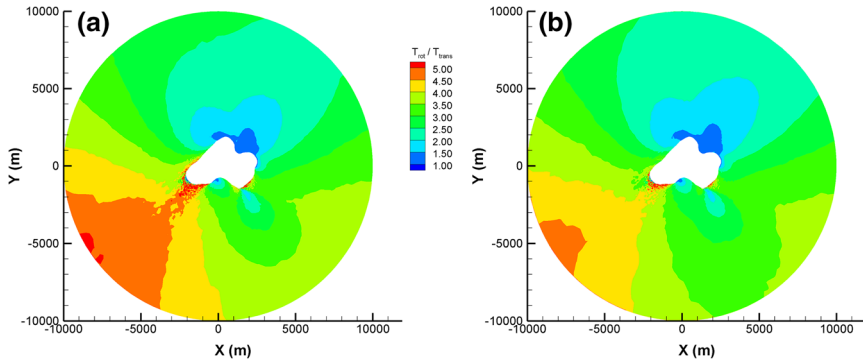


Fig. 25 Temperature ratio ($T_{\text{rot}}/T_{\text{trans}}$) distributions of the inner gas coma of **a** Case 0, and **b** Case 7

Acknowledgments This work has been supported by the Swiss National Science Foundation (SNSF) under Grant IZ32Z0_145126 8.

References

- A.A. Alexeenko, Elastic collision models in DSMC: a review and guide, in *Abstract, DSMC 2013 Conference* (2013)
- G.A. Bird, *Molecular Gas Dynamics and the Direct Simulation of Gas Flows* (Oxford University Press, Oxford, 1994)
- M.R. Combi, Time-dependent gas kinetics in tenuous planetary atmospheres: the cometary coma. *Icarus* **123**, 207–226 (1996)
- M.R. Combi, W.H. Smyth, Monte Carlo particle-trajectory models for neutral cometary gases. I—models and equations. *Astrophys. J.* **327**, 1026–1043 (1988)
- J.F. Crifo, G.A. Loukianov, A.V. Rodionov, G.O. Khanlarov, V.V. Zakharov, Comparison between Navier–Stokes and direct Monte-Carlo simulations of the circumnuclear coma. I. Homogeneous, spherical source. *Icarus* **156**, 249–268 (2002)
- J.F. Crifo, G.A. Loukianov, A.V. Rodionov, V.V. Zakharov, Navier–Stokes and direct Monte Carlo simulations of the circumnuclear coma II. Homogeneous, aspherical sources. *Icarus* **163**, 479–503 (2003)
- J.F. Crifo, G.A. Loukianov, A.V. Rodionov, V.V. Zakharov, Direct Monte Carlo and multifluid modeling of the circumnuclear dust coma. Spherical grain dynamics revisited. *Icarus* **176**, 192–219 (2005)
- S. Finklenburg, *Investigations of the Near Nucleus Gas and Dust Coma of Comets*. PhD thesis, University of Bern, Switzerland (2014)
- S. Finklenburg, N. Thomas, C.C. Su, J.S. Wu, The spatial distribution of water in the inner coma of Comet 9P/Tempel 1: comparison between models and observations. *Icarus* **236**, 9–23 (2014)
- N. Fougere, M.R. Combi, M. Rubin, V. Tenishev, Modeling the heterogeneous ice and gas coma of Comet 103P/Hartley 2. *Icarus* **225**, 688–702 (2013)
- N. Fougere, M.R. Combi, V. Tenishev, Global 3D kinetic model of cometary rarefied atmosphere toward a description of the coma of Comet 103P/Hartley 2, in *AAS/Division for Planetary Sciences Meeting Abstracts*, vol. 45, #413.21 (2013b)
- M.A. Gallis, J.R. Torczynski, D.J. Rader, G.A. Bird, Accuracy and convergence of a new DSMC algorithm, in *AIAA Paper*, 2008-3913 (2008)
- J. Greenwood, The correct and incorrect generation of a cosine distribution of scattered particles for Monte-Carlo modelling of vacuum systems. *Vacuum* **67**, 217–222 (2002)
- O. Groussin, J.M. Sunshine, L.M. Feaga, L. Jorda, P.C. Thomas, J.Y. Li, M.F. A’Hearn, M.J.S. Belton, S. Besse, B. Carcich, T.L. Farnham, D. Hampton, K. Klaasen, C. Lisse, F. Merlin, S. Protospapa, The temperature, thermal inertia, roughness and color of the nuclei of Comets 103P/Hartley 2 and 9P/Tempel 1. *Icarus* **222**, 580–594 (2013)
- S. Gulikis, M. Allen, P. Allmen, G. Beaudin, N. Biver, D. Bockelée-Morvan, M. Choukroun, J. Crovisier, B.J.R. Davidsson, P. Encrenaz, T. Encrenaz, M. Frerking, P. Hartogh, M. Hofstadter, W.H. Ip, M.

- Janssen, C. Jarchow, S. Keihm, S.W. Lee, E. Lellouch, C. Leyrat, L. Rezac, F.P. Schloerb, T. Spilker, Subsurface properties and early activity of comet 67P/Churyumov–Gerasimenko. *Science* **347**, 6220 (2015)
- M. Hässig, K. Altwegg, H. Balsiger, A. Bar-Nun, J.J. Berthelier, A. Bieler, P. Bochslers, C. Briois, U. Calmonte, M. Combi, J. De Keyser, P. Eberhardt, B. Fiethe, S.A. Fuselier, M. Galand, S. Gasc, T.I. Gombosi, K.C. Hansen, A. Jäckel, H.U. Keller, E. Kopp, A. Korh, E. Kührt, L. Le Roy, U. Mall, B. Marty, O. Mousis, E. Neefs, T. Owen, H. Rème, M. Rubin, T. Sémon, C. Tornow, C.Y. Tzou, J.H. Waite, P. Wurz, Time variability and heterogeneity in the coma of 67P/Churyumov–Gerasimenko. *Science* **347**, 6220 (2015)
- W.F. Huebner, J. Benkhoff, M.T. Capria, A. Coradini, C. De Sanctis, R. Orosei, D. Prialnik, *Heat and Gas Diffusion in Comet Nuclei* (ISSI/ESA Publications, Noordwijk, 2006)
- L. Jorda, R. Gaskell, S.F. Hviid, C. Capanna, F. Preusker, F. Scholten, P. Gutiérrez, Shape Models of 67P/Churyumov–Gerasimenko. RO-C-OSINAC/OSIWAC-5-67PSHAPE-V1.0. NASA Planetary Data System and ESA Planetary Science Archive (2015) (in preparation)
- H.U. Keller, C. Barbieri, P. Lamy, H. Rickman, R. Rodrigo, K.P. Wenzel, H. Sierks, M.F. A'Hearn, F. Angrilli, M. Angulo, M.E. Bailey, P. Barthol, M.A. Barucci, J.L. Bertaux, G. Bianchini, J.L. Boit, V. Brown, J.A. Burns, I. Büttner, J.M. Castro, G. Cremonese, W. Curdt, V. Da Deppo, S. Debei, M. De Cecco, K. Dohlen, S. Fornasier, M. Fulle, D. Germerott, F. Gliem, G.P. Guizzo, S.F. Hviid, W.H. Ip, L. Jorda, D. Koschny, J.R. Kramm, E. Kührt, M. Küppers, L.M. Lara, A. Llebaria, A. López, A. López-Jimenez, J. López-Moreno, R. Meller, H. Michalik, M.D. Michelena, R. Müller, G. Naletto, A. Origné, G. Parzianello, M. Pertile, C. Quintana, R. Ragazzoni, P. Ramous, K.U. Reiche, M. Reina, J. Rodríguez, G. Rousset, L. Sabau, A. Sanz, J.P. Sivan, K. Stöckner, J. Tabero, U. Telljohann, N. Thomas, V. Timon, G. Tomasch, T. Wittrock, M. Zaccariotto, OSIRIS—the scientific camera system Onboard Rosetta. *Space Sci. Rev.* **128**, 433–506 (2007)
- I.L. Lai, C.C. Su, W.H. Ip, C.E. Wei, J.S. Wu, M.C. Lo, Y. Liao, N. Thomas, Transport and distribution of oxygen atoms from H₂O photodissociation in the inner coma of comet 67P/Churyumov–Gerasimenko. *Earth Moon Planets* (2015) (this volume)
- S. Lee, P. von Allmen, L. Kamp, S. Gulkis, B.J.R. Davidsson, Non-LTE radiative transfer for sub-millimeter water lines in comet 67P/Churyumov–Gerasimenko. *Icarus* **215**, 721–731 (2011)
- S. Mottola, S. Lowry, C. Snodgrass, P.L. Lamy, I. Toth, A. Rožek, H. Sierks, M.F. A'Hearn, F. Angrilli, C. Barbieri, M.A. Barucci, J.L. Bertaux, G. Cremonese, V. Da Deppo, B. Davidsson, M. De Cecco, S. Debei, S. Fornasier, M. Fulle, O. Groussin, P. Gutiérrez, S.F. Hviid, W.H. Ip, L. Jorda, H.U. Keller, J. Knollenberg, D. Koschny, R. Kramm, E. Kührt, M. Küppers, L. Lara, M. Lazzarin, J.J. Lopez Moreno, F. Marzari, H. Michalik, G. Naletto, H. Rickman, R. Rodrigo, L. Sabau, N. Thomas, K.P. Wenzel, J. Agarwal, I. Bertini, F. Ferri, C. Güttler, S. Magrin, N. Oklay, C. Tubiana, J.B. Vincent, The rotation state of 67P/Churyumov–Gerasimenko from approach observations with the OSIRIS cameras on Rosetta. *Astron. Astrophys.* **569**, L2 (2014)
- K. Nanbu, Direct simulation scheme derived from the Boltzmann equation. I. Monocomponent gases. *J. Phys. Soc. Jpn.* **49**, 2042–2049 (1980)
- M. Rubin, N. Fougere, K. Altwegg, M.R. Combi, L. Le Roy, V.M. Tennishev, N. Thomas, Mass transport around comets and its impact on the seasonal differences in water production rates. *Astrophys. J.* **788**, 168 (2014)
- S.A. Sandford, L.J. Allamandola, The condensation and vaporization behavior of ices containing SO₂, H₂S, and CO₂: implications for IO. *Icarus* **106**, 478–488 (1993)
- Y.V. Skorov, G.N. Markelov, H.U. Keller, Direct statistical simulation of the near-surface layers of the cometary atmosphere. I. A spherical nucleus. *Sol. Syst. Res.* **38**, 455–475 (2004)
- Y.V. Skorov, G.N. Markelov, H.U. Keller, Direct statistical simulation of the near-surface layers of a cometary atmosphere. II: a nonspherical nucleus. *Sol. Syst. Res.* **40**, 219–229 (2006)
- Y.V. Skorov, H. Rickman, A kinetic model of gas flow in a porous cometary mantle. *Planet. Space Sci.* **43**, 1587–1594 (1995)
- Y.V. Skorov, H. Rickman, Gas flow and dust acceleration in a cometary Knudsen layer. *Planet. Space Sci.* **47**, 935–949 (1999)
- C.C. Su, *Parallel Direct Simulation Monte Carlo (DSMC) Methods for Modeling Rarefied Gas Dynamics*. PhD thesis. National Chiao Tung University, Taiwan (2013)
- C.C. Su, M.R. Smith, F.A. Kuo, J.S. Wu, C.W. Hsieh, K.C. Tseng, Large-scale simulations on multiple graphics processing units (GPUs) for the direct simulation Monte Carlo method. *J. Comput. Phys.* **231**, 7932–7958 (2012)
- V. Tennishev, M.R. Combi, B.J.R. Davidsson, A global kinetic model for cometary comae: the evolution of the coma of the Rosetta target Comet Churyumov–Gerasimenko throughout the mission. *Astrophys. J.* **685**, 659–677 (2008)

- V. Tenishev, M.R. Combi, M. Rubin, Numerical simulation of dust in a cometary coma: application to comet 67P/Churyumov–Gerasimenko. *Astrophys. J.* **732**, 104 (2011)
- M. Vargas, S. Stefanov, D. Valougeorgis, On the effect of the boundary conditions and the collision model on rarefied gas flows, in *AIP Conference Proceedings-American Institute of Physics*, vol. 1333, p. 354 (2011)
- W. Wagner, A convergence proof for Bird's direct simulation Monte Carlo method for the Boltzmann equation. *J. Stat. Phys.* **66**, 1011–1044 (1992)
- J.S. Wu, Y.Y. Lian, Parallel three-dimensional direct simulation Monte Carlo method and its applications. *Comput. Fluids* **32**, 1133–1160 (2003)
- J.S. Wu, K.C. Tseng, Parallel DSMC method using dynamic domain decomposition. *Int. J. Numer. Meth. Eng.* **63**, 37–76 (2005)
- J.S. Wu, K.C. Tseng, F.Y. Wu, Parallel three-dimensional DSMC method using mesh refinement and variable time-step scheme. *Comput. Phys. Commun.* **162**, 166–187 (2004)
- T. Ytrehus, *Kinetic Theory Description and Experimental Results for Vapor Motion in Arbitrary Strong Evaporation* (Von Karman Institute for Fluid Dynamics, Sint-Genesius-Rode, 1975)
- V.V. Zakharov, A.V. Rodionov, G.A. Lukianov, J.F. Crifo, Monte-Carlo and multifluid modelling of the circumnuclear dust coma II. Aspherical-homogeneous, and spherical-inhomogeneous nuclei. *Icarus* **201**, 358–380 (2009)
- S.W. Zhang, G.Z. Li, J. Han, The positional and angular distribution of molecules flowing through cylindrical tube in free molecular flow. *Phys. Procedia* **32**, 513–524 (2012)